Light Chain Dominant Quaternary Epitope Recognition and IgG3 Switching Drive Broad Dengue and Zika Virus Neutralization

Sanjeev Kumar[1,2,3,4,†,*], Connor A. P. Scott[5,6,†], Lingling Xu[1,2,3,†], Kathryn Moore[1,2,3,7], Jacob V. Velden[1,2,3,7], Samuel Shih[1,2,3], Richard H. West[1,2,3], Sneh Lata Gupta[1,2,3], Naphak Modhiran[5,6], Mehul S. Suthar[1,2,3,7,8], Daniel Watterson[5,6,*], Jens Wrammert[1,2,3,*]

[1]Division of Infectious Diseases, Department of Pediatrics, School of Medicine, Emory University, Atlanta, GA, USA

[2]Emory Vaccine Center, Emory University School of Medicine, Atlanta, GA, USA

[3]Centers for Childhood Infections and Vaccines, Children's Healthcare of Atlanta, Emory University, Department of Pediatrics, Department of Medicine, Atlanta, GA, USA

[4]Emory Vaccine Program, International Centre for Genetic Engineering and Biotechnology, New Delhi, India

[5]School of Chemistry and Molecular Biosciences, The University of Queensland St Lucia, Brisbane, Australia

[6]Australian Infectious Diseases Research Centre, Brisbane, Australia

[7]Emory National Primate Research Center, Atlanta, GA, USA

[8]Department of Microbiology and Immunology, Emory University, Atlanta, GA, USA

[†]These authors contributed equally to this work

[*]Co-corresponding authors: Sanjeev Kumar (sanjeev@icgeb.res.in); Daniel Watterson (d.watterson@uq.edu.au); Jens Wrammert (jwramme@emory.edu)

Keywords

DENV, ZIKV, neutralizing antibody, IgG subclass, cryo-EM

ABSTRACT

Defining how antibodies achieve broad neutralization across antigenically related flaviviruses could inform rational vaccine design. Here, we describe 3A06, a human monoclonal antibody isolated from a dengue-infected donor that potently neutralizes dengue virus serotypes 1-3 (DENV1-3) and Zika virus (ZIKV). Binding studies show that 3A06 selectively recognizes envelope (E) protein dimers, but not monomeric E, EDIII, or viral lysates, indicating strict dependence on a quaternary epitope. Affinity measurements reveal stronger binding to DENV1, DENV3, and ZIKV E dimers, with weaker binding to DENV2 and DENV4. High-resolution structural analysis of 3A06 Fab bound to a chimeric ZIKV particle shows that the antibody engages a quaternary epitope spanning three E protomers at the dimer interface. Strikingly, structural and functional analyses demonstrate that epitope recognition is dominated by the antibody light chain, with somatic mutations driving neutralization potency. While the IgG1 form neutralizes DENV1-3 and ZIKV, subclass switching to IgG3 enables neutralization of all four dengue serotypes. Structural studies using intact IgG3 with DENV support the hypothesis that the enhanced breadth is mediated by extended reach and flexibility of the IgG3 Fc-hinge scaffold. These results reveal a previously unrecognized class of flavivirus broadly neutralizing antibodies and demonstrate how antibody light chain and subclass architecture can be engineered to overcome viral diversity. Our findings provide a structural blueprint for the rational design of universal flavivirus vaccines.

INTRODUCTION

Flaviviruses such as dengue virus (DENV) and Zika virus (ZIKV) poses significant global health burden, with over 400 million infections annually, with no widely effective pan-serotype vaccine or therapeutics are currently available [1,2]. Antibody-mediated protection is a key focus for vaccine and therapeutic strategies, but concerns over antibody-dependent enhancement (ADE) and serotype-specific immunity have impacted the progress negatively [3,4]. The envelope (E) glycoprotein of flaviviruses, which mediates viral entry, is a major target of neutralizing antibodies (nAbs) [3,5–7]. While monomeric E protein has often been used in vaccines and diagnostics, recent studies suggest that E protein dimers, which are present as quaternary structure on mature flavivirus virions, represent more promising templates for rational vaccine design [3,4,8,9].

The E protein of flaviviruses exists in different conformational states during the viral life cycle, including a trimeric state together with the virally encoded pr chaperone in immature viral particles and as E dimers which assemble into the rafts of the mature infectious virions [10,11]. The majority of the existing monoclonal antibodies (mAbs) recognize epitopes on the monomeric form of E protein targeting its fusion loop epitope or EDIII domain [12]. However, a few antibodies that selectively engage the envelope dimer epitopes (EDE) formed on the dimeric form of E protein, the pre-fusion conformation on mature virions have recently been described [5,6,13–16]. Antibodies capable of binding such quaternary epitopes have shown increased breadth and potency in recent studies, suggesting that targeting of dimeric E-protein conformation on viral surface is a possible approach for designing universal flavivirus vaccine and therapeutics [5,14,15].

We previously identified several DENV and ZIKV nAbs from the plasmablasts of DENV2 infected donors. One of those nAbs 33.3A06 (described as 3A06 throughout this study) showed potent ZIKV neutralization despite being isolated from a DENV2 infected donor [7,12]. In this study, we comprehensively characterized 3A06 and found that it uniquely recognizes E dimers but not soluble E monomers. Furthermore, we show that antibody subclass architecture strongly influences neutralization breadth, as conversion to the IgG3 subclass enables expanded activity against all four dengue virus serotypes. Finally, 3A06 light chain is essential for epitope recognition of a quaternary epitope and viral neutralization as confirmed by cryo-electron microscopy (cryo-EM) based structural studies. The IgG3 version of 3A06 bound to flavivirus particles reveal how this antibody engages the virion surface in a bivalent manner, providing a structural explanation for its neutralization potency and subclass-

dependent activity. These results offer new insights into B cell immunity and antibody engineering or vaccine development strategies against flaviviruses.

77 **RESULTS**

78 **3A06 antibody selectively recognizes a quaternary E-protein dimer epitope**

79 We previously reported the discovery of a fully human monoclonal antibody (mAb) 3A06 from
80 the plasmablasts of a DENV2 infected donor #33 [7,12]. The 3A06 mAb neutralized ZIKV with
81 up to 45-fold higher potency than DENV1-3 serotypes, despite being originally isolated from
82 a DENV2 infected donor. To understand the epitope specificity, we first assessed its binding
83 profile using ELISA and biolayer interferometry. The 3A06 mAb binds to recombinant soluble
84 E (sE) protein dimers derived from DENV1-3 and ZIKV, but showed no binding to the
85 respective sE monomers, EDIII domain or viral lysates. This is similar to observations made
86 by others with EDE1-C10 and EDE2-A11 mAbs [5,6,13–16] (**Figures 1A and S1A-D**). Using a
87 live virus-based focus reduction neutralization test (FRNT) assays, we found that 3A06
88 showed slightly increased neutralization potency (0.07 – 0.1 µg/ml) against DENV1-3 viruses
89 as compared to EDE1-C10 (0.3 – 0.6 µg/ml) and EDE2-A11 (0.6 µg/ml) mAbs, but slightly
90 lower against ZIKV as compared to EDE1-C10 (**Figure 1B**). Octet biolayer interferometry
91 (BLI) analysis revealed a heterogenous interaction of 3A06 in the micromolar (2.62 µM) to
92 picomolar (1.78 pM) range against E-protein dimers (**Figure 1C**). These findings suggest that
93 3A06 targets a conformational epitope formed specifically in the dimeric assembly of the
94 envelope protein present on mature DENV and ZIKV viruses.

95 **Cryo-EM structure of 3A06 confirms recognition of a quaternary E-dimer epitope**

96 To understand the molecular basis of differences observed in 3A06 binding and neutralization
97 against DENV and ZIKV, we first determined the structure of 3A06 Fab. We used the Binjari
98 virus (BinJV) chimeric system [17–19], an insect-specific flavivirus, which accurately
99 recapitulates the architecture and antigenic landscape of pathogenic flaviviruses while
100 maintaining a high safety profile. The ZIKV structural proteins were presented on a Binjari
101 virus backbone (herein bZIKV), to generate chimeric virions suitable for high-resolution cryo-
102 EM analysis of 3A06 Fab binding. The 4.6 Å cryo-EM structure of bZIKV complexed with 3A06
103 Fab at 4°C showed that 3A06 binds a quaternary E-dimer dependent epitope across three E
104 protomers with 120 Fab fragments visible on the surface of the virion (**Figure 2A**). This
105 structure was further refined using symmetry expansion of the asymmetric unit to produce a
106 3.1 Å map that could then be modelled (**Figure 2B**). The atomic model of bZIKV complexed
107 with 3A06 Fab further highlighted the quaternary nature of the 3A06 epitope, showing
108 extensive hydrogen bonding across three E protomers per Fab fragment (**Figure 2C**). Within
109 the asymmetric unit, two 3A06 Fabs bind at the 2- and 3- fold axis respectively (**Figure 2C**).

110 Each Fab binds across EDI and EDIII of one E protomer, and EDII of the neighboring two
111 protomers, forming multiple bonds between the Fab and bZIKV (**Figure S2**). The VH of 3A06
112 buries 875 $Å^2$ across two E protomers making six hydrogen bonds between its HCDR2 and
113 HCDR3 loops and EDII of one E protomer and one hydrogen bond across to the neighboring
114 EDI. R109 in the HCDR3 loop forms a salt bridge with D71 in the bZIKV bc loop, a highly
115 conserved residue between ZIKV, and DENV serotypes 1-3. Notably, DENV4 contains an
116 alanine at position 71, which likely reduces the interaction strength of the 3A06 VH to DENV-
117 4. The VL of 3A06 buries 673 $Å^2$ with extensive hydrogen bonds between LCDR2 and EDIII
118 and EDI of one E protomer, LCDR1 and the fusion loop and bc loop of the neighboring E
119 protomer, and LCDR3 and the hi loop of the third E protomer. Interestingly, several key
120 hydrogen bonds for 3A06 to bZIKV were identified as low frequency mutations (2-10%) in the
121 germline mutation probability analysis (**Figure S3A, B**). S53, in the CDR-2 loop of 3A06 VL,
122 which forms a hydrogen bond with K373 on EDIII of bZIKV E protomer A, and N33 which
123 interacts with G104 of the E protomer C fusion loop. While G104 is highly conserved across
124 flaviviruses, K373 is not conserved among DENV serotypes and ZIKV, with DENV1, 2, and 3
125 having a proline, and DENV4 having a valine at the equivalent position. Overall sequence
126 conservation of the 3A06 epitope shows that the residues on EDII, including the FL, hi, and
127 bc loop contacted by the VH and VL are more conserved between DENV 1-4 and ZIKV
128 compared to the contacts facilitated by the light chain primarily on EDI and EDIII (**Figure S2**).
129 This structure highlights the importance of the VL in facilitating the potent neutralization of
130 3A06 for ZIKV. Further, the structure provides a mechanistic basis for its selective quaternary
131 epitope recognition.

132 **The neutralizing activity of 3A06 is primarily contributed by its light chain**

133 Building on our cryo-EM analysis showing that 3A06 engages a quaternary E-dimer epitope
134 with important role of the light chain, we next asked how somatic hypermutations (SHM) in
135 the heavy (VH) and light (VL) chain variable regions contribute to neutralization and virus
136 recognition. To address this, we generated antibodies in which VH, VL, or both were reverted
137 to their inferred germline sequences (iGL) as shown in (**Figure 3A**), allowing us to dissect the
138 relative contributions of each chain to antigen recognition and neutralization potency. The
139 iGLs were designed by reverting the VH or VL to their germline sequences but retaining the
140 original CDRH3 and CDRL3 sequences based on sequence alignments generated by IMGT
141 sequence analysis (**Figure S4**). Additionally, we evaluated the 3A06 antibody mutation
142 probabilities using ARMADiLLO, which is an online server to identify probable and improbable
143 mutations [20]. The improbable mutations are low-probability amino acid changes determined

144 by ARMADiLLO, which are amino acid substitutions in antibody variable regions that have a
145 low probability (2% or lower) of occurring during the natural somatic hypermutation process,
146 because they require multiple nucleotide changes [20]. Interestingly, the analysis resulted in the
147 identification of four improbable mutations in both the VH and VL genes ranging from 1-2%
148 frequency in the 3A06 antibody (**Figure S3A-B**). Based on these analyses we further
149 generated combinations of 3A06 VH and/or VL chain genes with only the improbable mutation
150 reverted to germline gene sequences (**Figure 3B**).

151 We observed that the variable light chain region-based iGL and Imp variant antibodies as
152 compared to variable heavy chain region-based variants play a significant role in antigen
153 recognition, as we observed reduced or negligible binding of these to DENV2 and ZIKV E-
154 protein dimers (**Figure 3C**). The VH reverted 3A06 IgG1 antibody showed 133.3% and 500%
155 reduction in ZIKV and DENV2 neutralization potential, respectively. However, the VL reverted
156 and VH-VL reverted iGL 3A06 antibodies showed no neutralizing activity against ZIKV or
157 DENV2 at all concentrations tested (**Figure 3D**). The VH-Imp reverted 3A06 IgG1 antibody
158 showed 133.3% and 1150% reduction in ZIKV and DENV2 neutralization potential,
159 respectively. In comparison, the VL-Imp reverted antibody showed more than a 10400%
160 reduction in neutralizing activity against DENV2 compared to wild-type 3A06 IgG1 antibody
161 (**Figure 3D**). The VH VL-Imp reverted 3A06 antibody showed greater than 8233.3% reduction
162 in neutralization against ZIKV. Against DENV2, the VH VL-Imp reverted 3A06 antibody did
163 not show any neutralization compared to the wild-type 3A06 IgG1 antibody (**Figure 3D**).
164 Moreover, the 3A06 iGL reverted or Imp reverted variant antibodies mediated enhancement
165 of DENV2 and ZIKV infection at sub neutralizing concentrations (**Figure 3E and 3F**). These
166 results revealed that 3A06 light variable gene is largely responsible for its potent ZIKV
167 neutralizing activity, and that improbable mutations contribute to its potent viral neutralizing
168 activity.

169 **3A06 is encoded by a unique antibody variable gene configuration**

170 Our structural and functional analyses showing that 3A06 engages a quaternary E-dimer
171 epitope with dominant light-chain contacts and that neutralization largely depends on the light
172 chain, we next investigated the genetic basis of these properties. Sequence analysis of the
173 variable regions revealed that 3A06 is encoded by a rare combination of heavy and light chain
174 immunoglobulin genes not commonly observed among other flavivirus broadly neutralizing
175 antibodies, including those targeting EDE1 (EDE1-C8, C10), EDE2 (EDE2-B7, A11), or other
176 quaternary epitopes (SIgN-3C) (**Table 1 and Figure S4**). The heavy chain variable region is

177 derived from IGHV4-61*01, IGHD4-17*01, and IGHJ5*01, while the light chain derived from
178 IGLV1-44*01, IGHJ3*01 gene. 3A06 heavy chain exhibits moderately high levels of somatic
179 hypermutation (11.34%) compared to previously reported E-dimer specific mAbs. The light
180 chain is somewhat less mutated (6.32%). 3A06 has a CDR3 (complementarity-determining
181 region 3) length of 18 amino acids, and 11 amino acids in CDRL3 region, which are
182 comparable to EDE1 specific antibodies EDE1-C10 and EDE1-C8 [5]. The rare IGHV/IGLV
183 combination positions the light chain CDRs to dominate contacts with the quaternary E-dimer
184 epitope, explaining the light-chain-driven recognition observed structurally and the
185 neutralization profile revealed in functional assays.

186 **3A06 IgG3 subclass broadens neutralization against dengue and zika viruses**

187 We next investigated how antibody subclass influences functional breadth. While the IgG1
188 form effectively neutralizes DENV1-3 and ZIKV, it fails to neutralize DENV4. To determine
189 whether Fc architecture could modulate this activity, we generated IgG2, IgG3, and IgG4
190 variants and assessed their neutralization profiles across all four dengue serotypes (**Figure**
191 **4A**). In contrast to 3A06 IgG1, its IgG3 version showed higher binding to sE protein dimers of
192 all four DENV serotypes and ZIKV (**Figure 4B and Figure S5A**) and potent neutralization
193 activity against DENV4 (**Figure 4C**), which was resistant to neutralization by 3A06 IgG1.
194 Further, to assess the potential for 3A06 mediated antibody-dependent enhancement (ADE),
195 we performed DENV2 and ZIKV infection assays using Fcγ receptor expressing U937 cells
196 pre-incubated with varying concentrations of 3A06 in various Fc variants. The 3A06 IgG1
197 variant mediated moderate enhancement of DENV2 and ZIKV infection at sub neutralizing
198 concentrations (**Figure 4D**). In contrast, the IgG3 version induced higher levels of DENV2
199 and ZIKV ADE. The IgG2 subclass antibody didn't mediate enhancement, consistent with its
200 low affinity for Fcγ receptors [21,22].

201 Based on these observations, we next engineered the L234A/L235A/P329G (LALA-PG) Fc
202 variant of the 3A06 antibody in both IgG1 and IgG3 subclasses. The LALA-PG Fc mutant is
203 well-known to abrogate Fcγ receptor binding in IgG1, and here we grafted the same mutations
204 into IgG3 to determine whether these could also Fcγ receptor binding in the IgG3 version. We
205 did not observe any change in neutralization activity between the LALA-PG IgG1 and IgG3
206 antibodies and their respective wild-type antibodies (**Figure 4C**). As expected, IgG1 LALA-
207 PG antibody completely eliminated ADE. Interestingly, the same mutations incorporated into
208 the IgG3 version were also effective in silencing ADE (**Figure 4D**). These findings suggest

209 that 3A06 IgG subclasses and Fc variants can modulate epitope accessibility, and antigen-
210 antibody engagement dynamics.

211 **3A06 IgG3 hinge architecture enables bivalent virion engagement**

212 In order to understand the unique capacity of 3A06 to bind and neutralize DENV4 when
213 presented on IgG3 backbone, we performed cryo-EM with whole IgG3 for DENV2 and DENV4
214 and compared to ZIKV and DENV2 complexed with 3A06 Fab. Whole IgG3 format mAbs were
215 purified by protein G and complexed with virions. Cryo-EM datasets were collected and
216 complexes resolved by SPA. Comparing the resulting maps, the antibody density was the
217 lowest for DENV2 complexed with 3A06 Fab, followed by DENV4 3A06 IgG3, DENV2 3A06
218 IgG3 and ZIKV 3A06 (**Figure 5A**), consistent with the observed binding levels. Similar to
219 ZIKV, no antibody density was observed at the 5-fold proximal site, which results from a clash
220 across the E rafts, and this configuration also abrogates the intra-dimer LC contacts critical
221 for 3A06 binding. Although the occupancy was improved for the DENV2 bound to intact IgG3
222 over Fab alone, no clear Fc or hinge density was observed, most likely due to the inherent
223 flexibility of these regions. Interestingly, extra density around the CH1 and CL domains was
224 observed for DENV2 complexed with 3A06 IgG3 when compared to ZIKV and Fab (**Figure**
225 **5B, green**). In order to examine this in more detail, focused classification was carried out
226 using symmetry expanded particle sets, focusing on either side of the CH1 and CL domains
227 (**Figure 5B dashed circles**). This revealed two distinct classes, where the Fab densities at
228 the 3-fold proximal site can adopt either a conformation with the CH1 and CL domains bent
229 over towards the adjacent 2-fold position within the E raft (**Figure 5C, class 1**) or a
230 conformation similar to the 2 -fold site Fab (**Figure 5C, class 2**). These two conformations
231 alter the relative positions of the CH1 linker region and therefore influence the potential for
232 bivalent engagement of the full antibody molecule (**Figure 5D, Figure S6**). Notably, we
233 observed Fab densities at the 2-fold position (intra-raft) in both classifications, while the
234 antibody density at the adjacent 3-fold position (inter-raft) was stronger in the 2nd class,
235 consistent with the ability of the IgG3 to bind across the E rafts when in this more favorable
236 CH1 CL conformation. This is different to what has been previously observed for DENV mAb
237 C10 when complexed with virions as a F(ab)2' [23], where only a single bivalent binding mode
238 was observed with C10 adopting a conformation similar to our observed Class 1, but with no
239 clear densities at the 2-fold sites. To examine this difference further, we investigated the
240 relative distances of the first disulfide position of the hinge for C10 and 3A06 in IgG1 and IgG3
241 framework (**Figure S7**). We found that the disulfide is least favorable for 3A06 in IgG1,
242 followed by C10, while in IgG3 format 3A06 is easily able to retain the hinge disulfide whilst

243 simultaneously engaging both 3-fold proximal epitopes within the raft. Overall, these findings
244 suggest that 3A06 in IgG3 format, due to its extended hinge allows bivalent engagement of
245 the virion in multiple configurations, leading to enhanced binding and neutralization.

246 **DISCUSSION**

247 The comprehensive characterization of 3A06 as a quaternary E-dimer conformation specific
248 human monoclonal antibody with potent DENV and ZIKV cross-neutralizing capacity offers
249 several conceptual advances. First, it advances the existing knowledge that heavy chain
250 dominated paratopes primarily determine antigen specificity in anti-flavivirus antibodies. In
251 the case of 3A06, we find that antigen binding, affinity, and neutralization potency are critically
252 dependent on the light chain, as confirmed by functional assays based on chimeric constructs
253 encoding iGL variants and improbable mutations reverted 3A06 antibody variants. Such light
254 chain dominated interactions have rarely been observed in flavivirus immunity and could open
255 new avenues for epitope focused flavivirus vaccine design and antibody optimization
256 strategies.

257 Our observations of the impact of IgG subclass in modulating both neutralization breadth and
258 ADE potential of 3A06 adds an important finding to the understanding of antibody-antigen
259 interaction. While IgG1 broadly neutralizes DENV1-3 and ZIKV, only the IgG3 version
260 uniquely neutralizes DENV4, a serotype often resistant to many broadly neutralizing
261 antibodies. This may be explained by the unique structural features of the IgG3 constant
262 region, such as its flexible and longer hinge region, which can improve epitope engagement
263 or accessibility and favor bivalent binding. This was consistent with our cryo-EM studies of
264 intact 3A06 IgG3 with DENV virions, where movement of the CH1 and CL domains within the
265 3-fold Fab region allowed alternate bivalent binding of both intra and inter-raft epitopes. This
266 is different to what has been previously observed for C10, where only a single class of intra-
267 raft 3 to 3-fold binding was resolved [23]. These unique properties of the IgG3 likely enhance
268 the functional interaction of the antibody with the complex quaternary epitopes on DENV4.
269 Moreover, the neutralization breadth of C10 antibody is governed by epitope topology on the
270 virion surface, whereas 3A06 breadth is enabled by antibody architectural flexibility,
271 suggesting that 3A06 defines a distinct quaternary epitope compared to the canonical EDE
272 recognized by C10 [16,23].

273 The rare germline gene usage of 3A06 further supports the idea that some of the most
274 effective broadly neutralizing antibodies arise from uncommon B cell lineages. The IGHV4-
275 61/IGLV1-44 combination observed here is underrepresented in known DENV/ZIKV
276 antibodies targeting the conformational epitopes present on the dimeric state of the E-protein.
277 This highlights the possibility that natural DENV infection resulted in induction of E-dimer
278 specific antibodies comprising different unbiased immunogenetic features. These findings

highlight the need for expanded profiling of underrepresented B cell clones and non-public clonotypes. The quaternary epitope recognized by 3A06 is present only on intact virions and is not reproduced by monomeric E protein, suggesting that vaccine antigens must preserve E-dimer organization to elicit similar antibodies.

In summary, our study defines a unique class of broadly neutralizing antibody, that target dimeric E-protein conformation via light chain dependent mechanisms to achieve potent cross-neutralization against DENV and ZIKV. We demonstrate the potential for IgG3 to facilitate the engagement of both intra and inter-raft epitopes in a bivalent mode. These findings demonstrate that antibody subclass architecture can directly influence viral epitope accessibility and neutralization breadth, revealing a previously underappreciated mechanism by which antibody structure shapes antiviral activity. Together, these results expand the known mechanisms of antibody mediated broad flavivirus neutralization and provide new templates for structure guided vaccine and therapeutics designed to tackle the DENV and ZIKV infection burden. These insights shift the focus of vaccine design from simple sequence conservation to the complex spatial requirements of the quaternary viral surface.

294 **METHOD DETAILS**

295 **Cell lines**

296 Vero CCL-81 cells (ATCC), were maintained in Eagle's Minimum Essential Medium (EMEM)
297 (ATCC) medium supplemented with 10% fetal bovine serum (FBS) (HyClone) and antibiotic-
298 antimycotic (1X) (Gibco). U937 cells (ATCC) were maintained in RPMI-1640 supplemented
299 with 10% FBS, 2mM L-Glutamine (Gibco), 1mM 4-(2-hydroxyethyl)-1-
300 piperazineethanesulfonic acid (HEPES) (Gibco), 1mM sodium pyruvate (Gibco), 1X Non-
301 essential Amino Acids (NEAA) (Gibco) and 1X penicillin/streptomycin (Gibco). All these cells
302 were cultured at 37°C with 5% CO_2. The expi293™ cells (Gibco) were maintained in expi293
303 expression medium (Gibco) and cultured at 37°C, 125 rpm shaking and 8% CO_2.

304 **DENV and ZIKV amplification and lysate preparation**

305 DENV1 strain WestPac74, DENV2 strain 16681, DENV3 strain 3001, DENV4 strain Sri Lanka
306 92 and ZIKV strain PRVABC59 was obtained from the Centers for Disease Control and
307 Prevention (CDC) and was passaged by infecting Vero CCL-81 cells at a multiplicity of
308 infection (MOI) of 0.1 in EMEM (ATCC). After a 1 h infection at 37°C, the virus inoculum was
309 removed and EMEM supplemented with 10% FBS and 1% antibiotic-antimycotic (1X) (Gibco)
310 was added to the cells. Upon observation of severe cytopathic effect (CPE) 4 to 6 days
311 (DENVs) and 48 hr for ZIKV, supernatants were collected and spun down at 4000 × g for 10
312 min at 4°C. Supernatant containing virus was supplemented with an additional 10% (vol/vol)
313 FBS before freezing at –80 °C. Viruses were titred by focus forming assay on Vero CCL-81
314 cells before use.

315 The viral lysates were prepared as described previously [7]. Briefly, to prepare all four DENV1-
316 4 serotypes and ZIKV lysates, the remaining Vero CCL81 adherent cells and cell pellet from
317 the virus-containing supernatant were washed twice with Dulbecco's Phosphate Buffer Saline
318 (DPBS) and then resuspended in the cell lysis buffer (10 mM Tris, 150 mM NaCl, 1% sodium
319 deoxycholate, 1% Triton X-100, pH 7.4) supplemented with protease inhibitor (Thermo Fisher
320 Scientific) and phosphatase inhibitor (Biovision). Mock lysate was prepared in a similar
321 fashion with uninfected cells. Bradford assay was performed to quantitate total protein yield.

322 **Dimeric DENV and ZIKV Env antigen expression and purification**

323 All four serotypes DENV1-4, and ZIKV dimeric Env constructs were designed by incorporating
324 dimer stabilizing disulfide bonds based on previous designs [3] with a c-terminal strep-tag II

325 sequence were synthesized and cloned in pTwist Beta Glo Neo expression vector from Twist
326 Biosciences. Transfections were performed as per the manufacturer's protocol in expi293
327 cells (Thermo Fisher). Briefly, expi293 cells were seeded at a density of $2x10^6$ cells/ml in
328 Expi293 expression medium and incubated at 37°C and 125 rpm with 8% CO_2 overnight. The
329 next day, $2.5x10^6$ cells/ml were transfected using ExpiFectamine™ 293 transfection reagent
330 (ThermoFisher). Next morning, enhancers 1 and 2 were added along with 0.5% of antibiotic-
331 antimycotic solution (Gibco). The cells continued to grow for 5 days at 37°C, 125 rpm, 8%
332 CO_2 incubator. The cells were removed by centrifugation at 6,000g for 20 minutes at room
333 temperature and dimeric env protein-containing supernatant was collected. The supernatant
334 was filtered through 0.45 um filter assembly (VWR) and loaded onto pre-washed Strep-
335 Tactin®XT 4Flow® resin (IBA Lifesciences) for affinity purification. Resin washed with 1x wash
336 Buffer (buffer W) containing 25mM Tris, 150mM NaCl and 1mM EDTA with pH 8.0 followed
337 by Env protein elution in elution buffer 1x BXT buffer (IBA). Eluted protein dialyzed against
338 DPBS and concentrated. The concentrated protein ran onto a Superdex200 Increase 10/300
339 column and protein eluted as dimeric Env collected.

340 **Monoclonal Antibody Expression and Purification**

341 Human mAbs used in study were generated as previously described [7,12]. First, 3A06, IgG
342 subclasses variants (IgG1, IgG2, IgG3 and IgG4) and IgG1 Fc variants, L234A/L235A/P329G
343 (LALA-PG) [24,25], were generated by replacing the constant region of the wild-type IgG1 heavy
344 chain expression vector with synthesized constructs (Twist Bioscience). The variable heavy
345 and light chain sequences of control antibodies EDE1-C10 [16], and EDE2-A11 [5] were
346 synthesized (Twist Bioscience) and cloned into human IgG1 expression vectors based on
347 PDB IDs 7A3N and 5N0A respectively. Next, the variable heavy and light chain sequences
348 encoding expression plasmids were transiently expressed in expi293F cells for 5 days and
349 secreted antibodies were purified from supernatants using protein A coupled sepharose
350 beads (Pierce) as per manufacturer's instructions.

351 **ELISA assays**

352 The binding potential of mAbs to ZIKV and DENV E protein antigens (Monomer, EDIII domain)
353 and viral lysates was determined by ELISA. Briefly, the recombinant DENV1-4, ZIKV antigens
354 and viral lysates were coated in separate Nunc Maxisorp ELISA plates (Thermo Scientific) at
355 a concentration of 1 µg/ml in DPBS overnight at 4°C. Next morning, the plates were washed
356 thrice with DPBS containing 0.05% Tween-20 (DPBST) and blocked with DPBST containing
357 1% BSA (ELISA buffer) for 1.5 hr at room temperature. Then, mAbs with serial 3-fold dilution

358 in ELISA buffer, starting at 10 µg/ml concentration were added to the plates and incubated at
359 room temperature for 1.5 h. The plates were washed thrice with DPBST, and the IgG signals
360 were detected by incubating with peroxidase-conjugated anti-human IgG (Jackson
361 ImmunoResearch) for 1 h. The plates were washed thrice with DPBST and developed using
362 an o-phenylenediamine substrate (Sigma) in 0.05M phosphate-citrate buffer (Sigma Aldrich)
363 containing 0.012% hydrogen peroxide. The absorbance values were measured at O.D. 490
364 nm. The absorbance values were plotted against the concentration of antibodies.

365 DENV and ZIKV E-protein dimer-based ELISA assays were performed using StrepTactinXT
366 coated plates. StrepTactinXT coated microplates (IBA lifesciences) do not require any
367 functionalization or blocking steps prior to protein immobilization. Briefly, 100 µL of Strep-
368 Tagged purified E-protein dimers in ELISA buffer at 1 µg/mL concentration were dispensed
369 in the corresponding wells for protein immobilization by a 2 h incubation at room temperature.
370 Following a triple wash with DPBST to remove unbound proteins, three-fold serial dilutions of
371 test mAbs and control mAbs (EDE1-C10, EDE2-A11, Z004 and 4G2) starting at 10 µg/ml
372 concentration in ELISA buffer were added and incubated for 1.5 h at room temperature. After
373 3 washes with DPBST, peroxidase-conjugated anti-human IgG (Jackson Immunoresearch)
374 diluted 1:3000 in ELISA buffer was added and incubated for 1 h, followed by three washes
375 with DPBST. Plates were developed with o-phenylenediamine substrate (Sigma-Aldrich) in
376 0.05 M phosphate-citrate buffer (Sigma-Aldrich) pH 5.0, containing 0.012% hydrogen
377 peroxide (Thermo Fisher Scientific). Absorbance was measured at 490 nm to obtain the
378 binding data.

379 **Octet BLI analysis**

380 Octet biolayer interferometry (BLI) was performed using an Octet Red96 instrument (ForteBio,
381 Inc.). Briefly, mAbs were captured on ProA biosensors at 5 µg/ml concentration in BLI running
382 buffer (0.1% BSA, 0.001% Tween20 in 1x DPBS). Binding kinetics were tested with serial 2-
383 fold serially diluted DENV1-4 and ZIKV E-protein dimers (100 nM to 6.25 nM). The baseline
384 was obtained by measurements taken for 120 s in BLI running buffer. The biosensors were
385 dipped to obtain association phase for 300 s in wells containing serial dilutions of E-protein
386 dimers. Then, the sensors were immersed in BLI running buffer for as long as 600 s to
387 measure the dissociation phase. Sensors were regenerated in glycine pH 2.0 buffer and
388 immediately neutralized by dipping in Tris pH 9.0 buffer. The mean K_{on}, K_{off} and apparent KD
389 values of the mAbs binding affinities for E-protein dimers were calculated from all the binding

390 curves based on their global fit to a 1:1 Langmuir binding model using Octet software version
391 12.0.

392 **Preparation of 4G2 Antibody**

393 Pan-flavivirus anti-envelope mAb 4G2 was isolated from the supernatant of mouse hybridoma
394 (D1-4G2-4–15; ATCC) grown in hybridoma medium (Thermofisher Scientific), and purified
395 using protein G beads (Pierce) according to the manufacturer's recommendations. The
396 antibodies were stored in 1x PBS for in-vitro cell culture assays and with 0.05% sodium azide
397 at 4°C for the binding assays.

398 **Live virus-based focus reduction neutralization test (FRNT) assays**

399 The neutralization potential of mAbs and serum samples was determined by FRNT as
400 described previously [7] with a few modifications. Two-fold serially diluted mAbs starting at
401 20 µg/ml concentration were incubated with a previously titrated amount of virus (~100 focus
402 forming units) of ZIKV or DENV1-4 for 1 h at 37 °C. Vero CCL81 cell monolayers in 96-well
403 plates were subsequently infected with the mixture for 1 h at 37 °C. An overlay containing 1%
404 (wt/vol) methylcellulose (Sigma) was added to the cells. After 48 h (ZIKV) and 72 h (DENV)
405 incubation at 37 °C, the cells were washed and fixed with a 1:1 mixture of acetone and
406 methanol at room temperature. Foci were stained using 4G2 at 0.5 µg/ml concentration for 2
407 h at room temperature followed by HRP-linked anti-mouse IgG (Cell Signaling) for 1 h and
408 developed using TrueBlue Peroxidase substrate (KPL) for 2 h at room temperature. At each
409 step, plates were washed thrice with 1x DPBS and Foci were imaged using a CTL-
410 Immunospot S6 Micro Analyzer.

411 **Antibody Dependent Enhancement (ADE) assay**

412 ADE assay was performed as described previously [7]. Briefly, serially diluted mAbs were
413 incubated with ZIKV with an MOI of 0.5 for 1 h at 37 °C. The immune complexes were added
414 in a 96-well plate containing $2x10^4$ U937 cells (ATCC) per well in RPMI-1640 with 10%
415 (vol/vol) FBS. The Cells were infected for 24 h at 37 °C. The cells were then washed and
416 fixed/permeabilized using BD intracellular staining reagents Fix/Perm Solution (BD
417 biosciences) and Perm/Wash Buffer (BD biosciences) according to the manufacturer's
418 protocol. Cells were stained with in-house prepared 4G2 antibody conjugated to Alexa fluor
419 594 for 1h for 25 min. The percentage of infected ($4G2^+$) cells was determined using flow

420 cytometry using the Cytek Aurora flow cytometer followed by analysis using FlowJo software
421 v10.

422 **Virus and antibody purification for Cryo-EM**

423 Chimeric viruses containing the non-structural genes of Binjari virus (BinJV) and prME genes
424 of ZIKV (Natal, Genbank: NC_035889)), DENV-2 (ET300, Genbank: EF440433), and DENV-
425 4 (ET288, Genbank: EF440435) were generated using circular polymerase extension
426 reaction as previously described [17,18,26]. To ensure mature virion preparations the prM furin
427 cleavage site of DENV-2 and DENV-4 prME was modified to an Influenza H5 HA furin
428 cleavage site (RERRRKKRS). Virus recovered from transfected C6/36 cells were passaged
429 to P1 and propagated in C6/36 cells (MOI: 0.1). Clarified viral supernatant was then purified
430 as previously described with PEG precipitation, followed by a 20% sucrose cushion, and 25-
431 40% potassium tartrate gradient [19,27]. Gradient fractions containing virus were then harvested
432 and used for Cryo-EM imaging. Fab fragments of 3A06 were generated by cloning the HV
433 region of 3A06 into a mammalian expression vector containing a C-terminal C-Tag (EPEA)
434 [28,29]. Plasmids encoding the HV Fab and LC were then transfected into ExpiCHO cells,
435 incubated for 7 days at 37 °C shaking, with the clarified supernatant then purified using an
436 CaptureSelect™ C-tagXL Pre-packed Column on an AKTA-Pure FPLC.

437 **Cryo-electron microscopy**

438 Chimeric flavivirus were complexed with excess 3A06 Fab fragments or IgG3 for 1 hour at
439 4 °C before being applied to glow discharged R3.5/1 holey carbon grids (Quantifoil). Grids
440 were then vitrified using an EM GP2 (Leica Microsystems) set at 4 °C and 95% relative
441 humidity, grids were pre-blotted for 10 secs, followed by blotting for 3 secs and immediately
442 plunge-frozen in liquid ethane. Grids were transferred under liquid nitrogen to a CRYO
443 ARM™ 300 (JEOL JEM-Z300FSC) transmission electron microscope operated at 300 kV,
444 equipped with a K3 direct electron detector (Gatan) and an omega in-column energy filter
445 operated at 20 eV (JEOL). Movies were recorded using SerialEM at 60,000 x magnification
446 [30].

447 **Cryo-EM processing, single particle analysis, and model building**

448 Cryo-EM datasets were motion corrected, and the contrast transfer function (CTF)
449 parameters were estimated using *cis*TEM [31]. Virus-Ab particles were automatically picked,
450 extracted, and classified over multiple rounds of 2D classification. The initial 3D

reconstructions on *cis*TEM were caried out ab initio, followed by 3D refinement using the low-resolution ab into model as a reference. High-resolution asymmetric focused reconstructions were carried out by symmetry expansion using *cis*TEM as previously described [19,32]. Each image was subtracted 60 times using each of the 60 icosahedral ASUs generating a dataset of isolated asymmetric units which were automatically centred. The dataset of ASUs was then further refined using *cis*TEM without symmetry applied. The initial atomic model of bZIKV complexed with 3A06 Fab was generated using an existing cryoEM structure of ZIKV virus (PDB: 6CO8) as a template with an AlphFold3 generated model of 3A06 Fab. All modelling was performed using iterative cycles of ISOLDE (v. 1.2.1), COOT (v.0.8.9.2), and PHENIX (v.1.19.2) [33–35]. The geometry and quality of the model were evaluated through a combination of PHENIX and the wwPDB Validation system.

Immunogenetic analyses of antibody genes

The immunogenetic analysis of both heavy chain and light chain germline assignment, framework region annotation, determination of somatic hypermutation (SHM) levels (nucleotides) and CDR loop lengths (amino acids) was performed with the aid of IMGT/HighV-QUEST (www.imgt.org/HighV-QUEST) [36,37].

Statistical analysis

Graphpad Prism version 9.0 was used for all statistical analyses.

DATA AND MATERIALS AVAILABILITY

All data needed to evaluate the conclusions in the paper are present in the paper and/or the Supplementary Materials. For materials requests, please reach out to the corresponding author(s).

ACKNOWLEDGEMENTS

We thank the cryo-EM data sets collected by Australia team. We thank Queensland staff members for their support in data collection.

FUNDING

This work was funded in part by NIH/National Institute of Allergy and Infectious Diseases (NIAID) Grants R01AI149486 (to J.W. and M.S.S.), R56AI110516 (to M.S.S.) and DBT/Wellcome Trust India Alliance Early Career Fellowship grant IA/E/18/1/504307 (to S.K.).

AUTHOR CONTRIBUTIONS

Conceptualization, S.K., D.W., and J.W.; methodology, S.K., N.M., M.S.S., D.W., J.W.; investigation, S.K., C.A.P.S., L.X., K.M., J.V.V., S.S., R.H.W., S.L.G., N.M.; visualization, N.M., M.S.S., D.W., J.W.; funding acquisition, S.K., M.S.S., D.W., J.W.; project administration, S.K., L.X., R.H.W.; supervision, M.S.S., D.W., J.W.; writing – original draft, S.K., C.A.P.S., M.S.S., D.W. and J.W.; writing – review & editing, all authors.

DECLARATION OF INTERESTS

All other authors declare no competing interests.

488 **FIGURES & FIGURE LEGENDS**

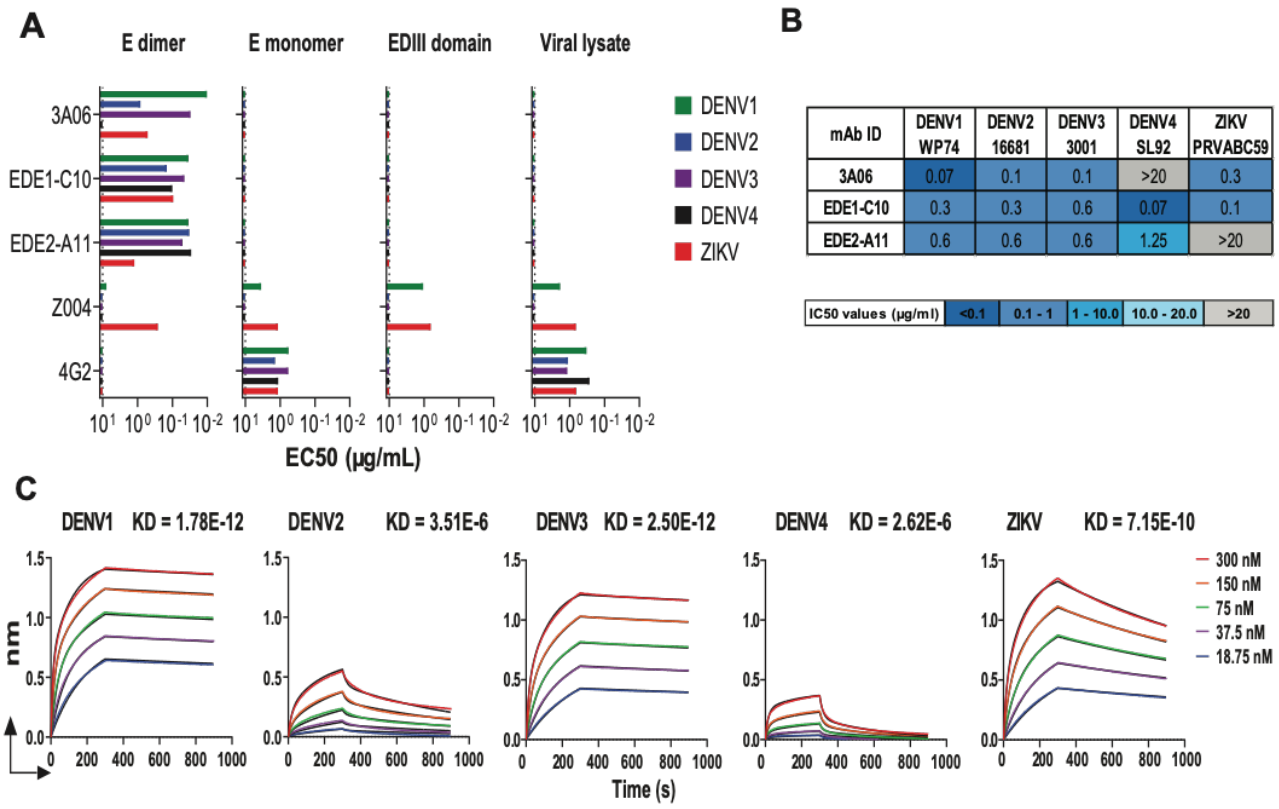

mAb ID	DENV1 WP74	DENV2 16681	DENV3 3001	DENV4 SL92	ZIKV PRVABC59
3A06	0.07	0.1	0.1	>20	0.3
EDE1-C10	0.3	0.3	0.6	0.07	0.1
EDE2-A11	0.6	0.6	0.6	1.25	>20

IC50 values (µg/ml)	<0.1	0.1 - 1	1 - 10.0	10.0 - 20.0	>20

489

490 **Figure 1: 3A06 antibody recognizes E protein dimers but not monomers. (A)** ELISA
491 binding. **(B)** Octet BLI analysis. **(C)** 3A06 neutralization analysis by live-virus based FRNT
492 assay.

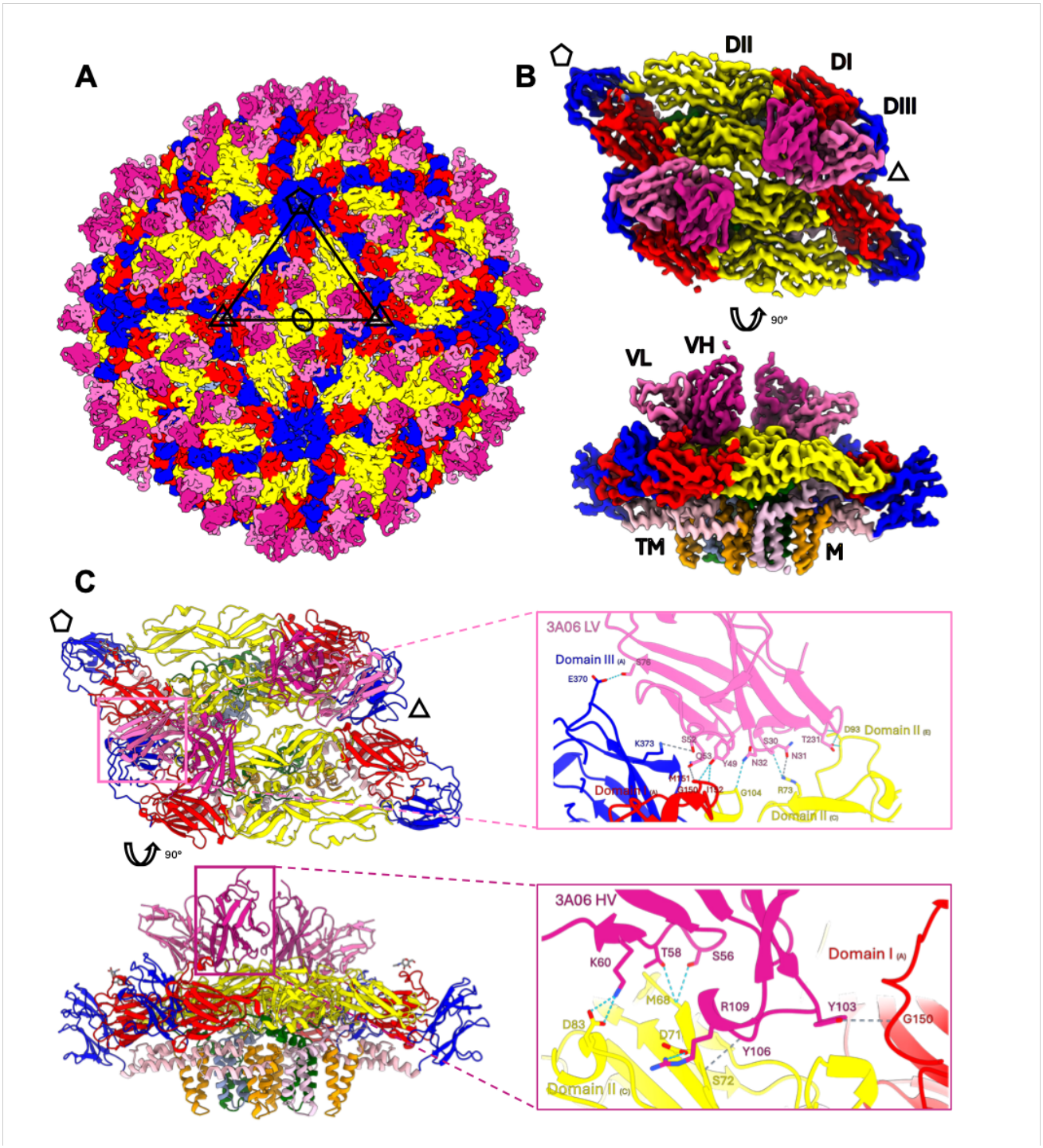

Figure 2: Cryo-EM structural analysis of 3A06 Fab in complex with DENV2-BinJV and ZIKV-BinJV. (A) 4.6 Å cryo-EM reconstruction of bZIKV complexed with 3A06 Fab colored by E domains (EDI: Red, EDII: Yellow, EDIII: Blue) and Fab heavy variable (Magenta) and light variable (Pink) domains. The asymmetric unit of bZIKV is labelled with the ellipses, triangles and pentagon representing the 2-, 3- and 5-fold icosahedral axes. (**B)** 3.1 Å symmetry expanded reconstruction of a pair of bZIKV E-M heterodimers complexed with 3A06 Fab. Density has been zoned to atomic model in panel C to display key contact sites

for two fab fragments. **(C)** Top and side view of atomic model of bZIKV complexed with 3A06 Fab with insets highlighting key hydrogen bonds for 3A06 LV (pink) and 3A06 HV (magenta).

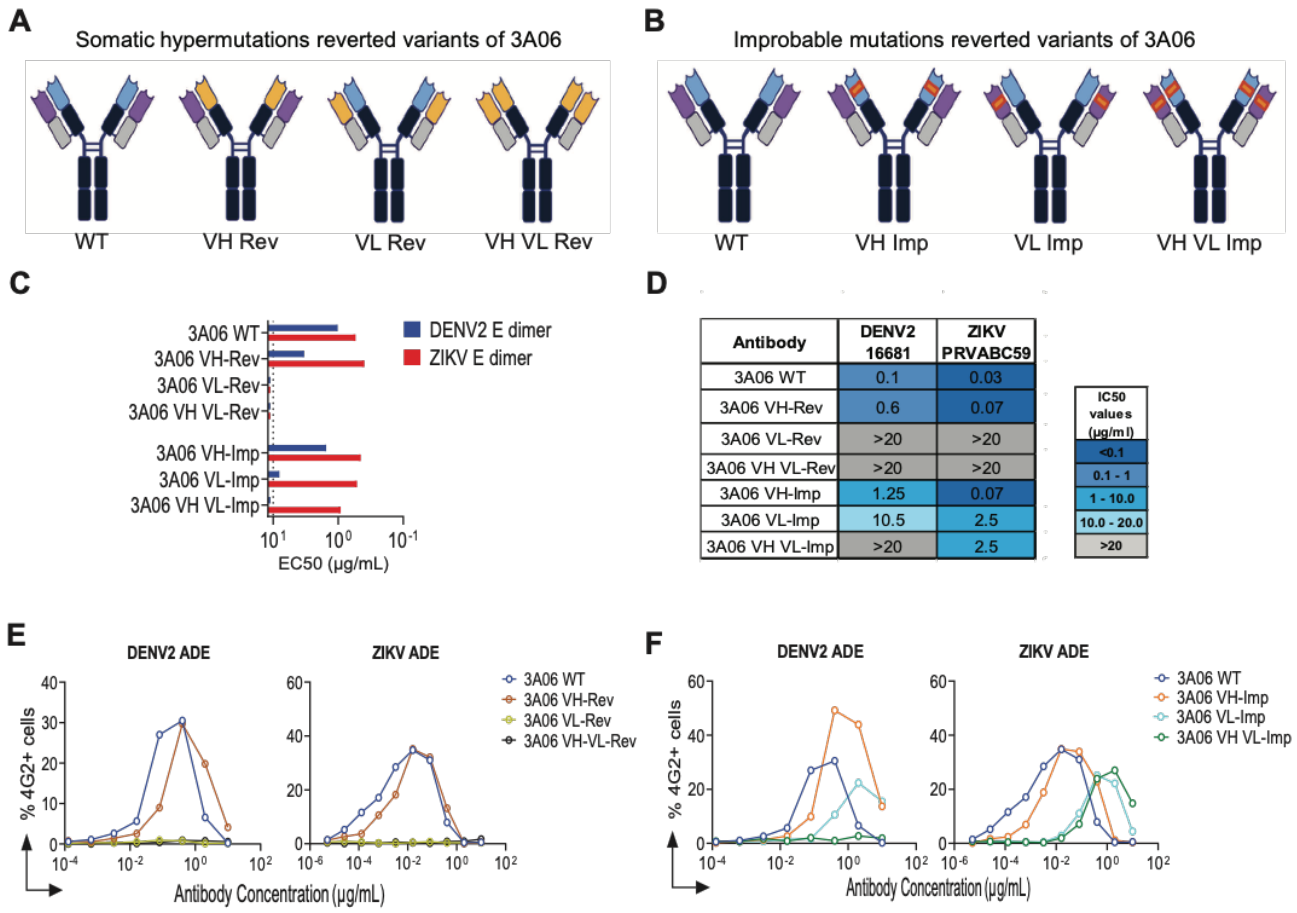

Figure 3: Neutralizing activity of 3A06 is primarily contributed by its light chain. (A) Structural presentation of 3A06 WT and its somatic hypermutation reverted iGL variants, variable heavy chain gene reverted VH-Rev, variable light chain gene reverted VL-Rev and both variable heavy and light chain genes reverted VH VL-Rev antibodies. **(B)** Representation of 3A06 WT and its improbable mutations reverted Imp variants, variable heavy chain gene reverted VH-Imp, variable light chain gene reverted VL-Imp and both variable heavy and light chain genes reverted VH VL-Imp antibodies. **(C)** ELISA binding of 3A06 iGL and Imp antibodies. **(D)** 3A06 iGL and Imp antibodies neutralization analysis by live-virus based FRNT assay. **(E)** In-vitro ADE analysis of 3A06 variants against DENV2 and ZIKV using U937 cells.

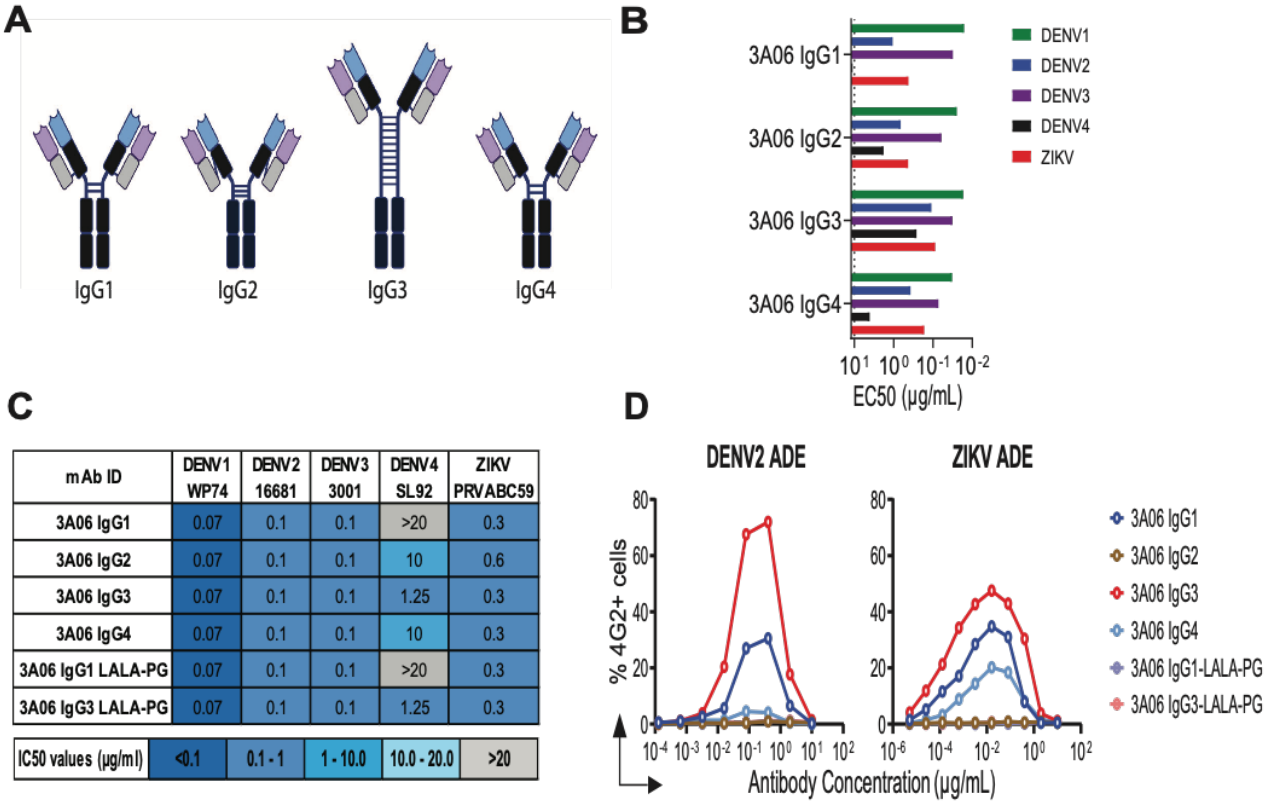

mAb ID	DENV1 WP74	DENV2 16681	DENV3 3001	DENV4 SL92	ZIKV PRVABC59
3A06 IgG1	0.07	0.1	0.1	>20	0.3
3A06 IgG2	0.07	0.1	0.1	10	0.6
3A06 IgG3	0.07	0.1	0.1	1.25	0.3
3A06 IgG4	0.07	0.1	0.1	10	0.3
3A06 IgG1 LALA-PG	0.07	0.1	0.1	>20	0.3
3A06 IgG3 LALA-PG	0.07	0.1	0.1	1.25	0.3

IC50 values (µg/ml)	<0.1	0.1 - 1	1 - 10.0	10.0 - 20.0	>20

Figure 4: 3A06 IgG3 antibody subclass version potently neutralizes DENV4. (A) Structural presentation of IgG1, IgG2, IgG3 and IgG4 subclass antibodies. **(B)** ELISA binding of 3A06 IgG subclasses. **(C)** 3A06 neutralization analysis by live-virus based FRNT assay. **(D)** In-vitro ADE analysis of 3A06 IgG subclasses against DENV2 and ZIKV using U937 cells.

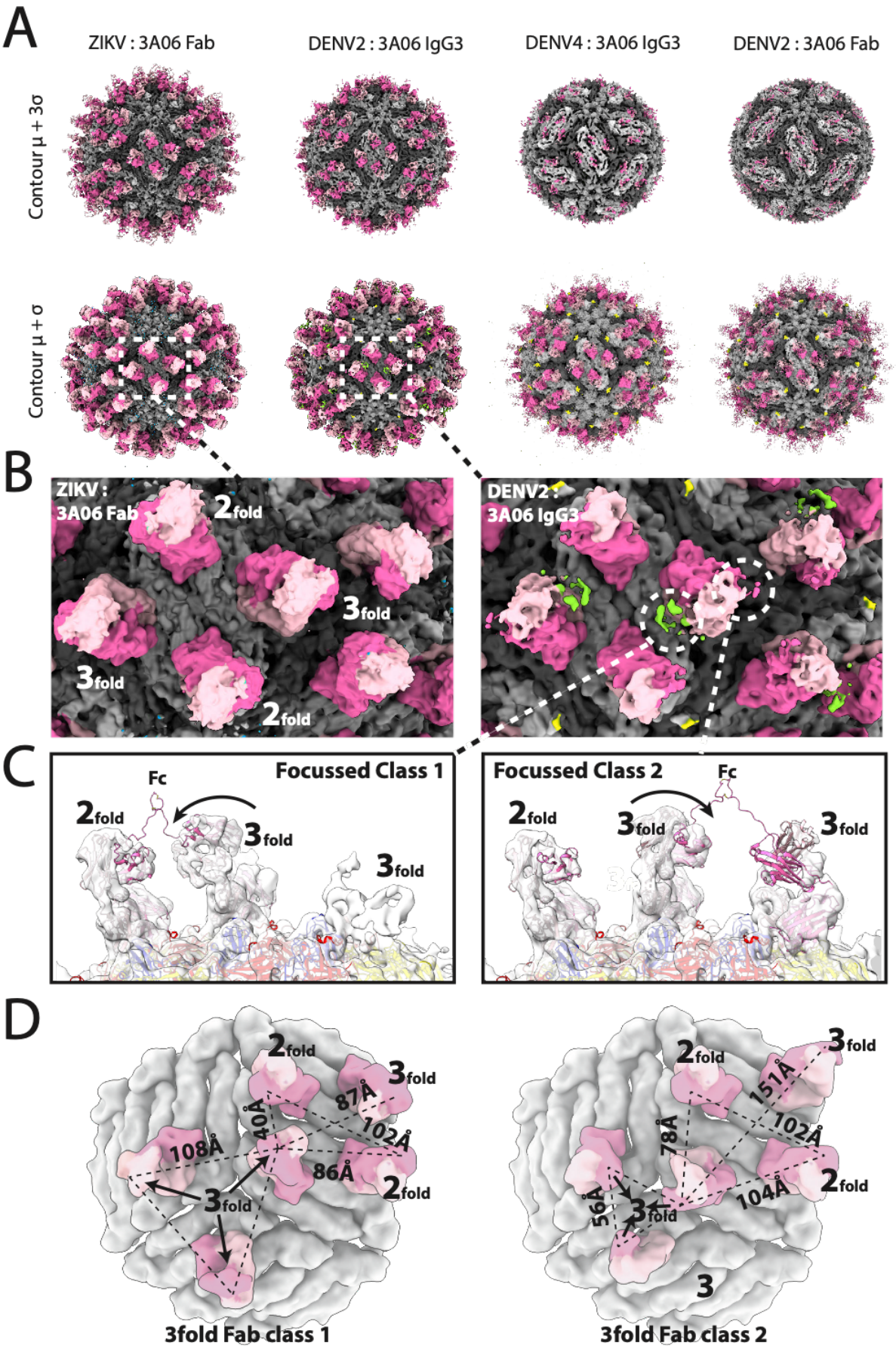
A
ZIKV : 3A06 Fab
DENV2 : 3A06 IgG3
DENV4 : 3A06 IgG3
DENV2 : 3A06 Fab
Contour μ + 3σ
Contour μ + σ
B
ZIKV :
3A06 Fab
2fold
3fold
3fold
2fold
DENV2 :
3A06 IgG3
C
Focussed Class 1
Fc
2fold
3fold
3fold
Focussed Class 2
Fc
2fold
3fold
3fold
D
2fold
3fold
87Å
40Å
102Å
108Å
86Å
2fold
3fold
3fold Fab class 1
2fold
3fold
151Å
78Å
102Å
56Å
3fold
104Å
2fold
3
3fold Fab class 2

518

519 **Figure 5: Cryo-EM structural analysis of 3A06 IgG3 complexed with DENV2 and DENV4.**
520 **(A)** Whole virion maps of bZIKV complexed with 3A06 Fab, bDENV2 complexed with intact
521 3A06 IgG3, bDENV-4 with intact 3A06 IgG3 and bDENV-2 complexed with 3A06 Fab. Virions
522 colored in greys representing the 3 E proteins in the asymmetric unit, with the 3A06 HC in
523 magenta and LC in pink. 2 different contour levels (mean+3σ top, mean+ σ below) are shown
524 for each reconstruction to highlight the occupancy differences of 3A06 for each complex**. (B)**
525 Close up view of the 3A06 densities shown for bZIKV:Fab (left) and bDENV2:IgG3 (right).
526 Additional densities observed only in the DENV2 IgG3 bound map are colored yellow for the
527 position of the N67 DENV glycan and green for an extra density adjacent to the 3-fold Fab
528 constant domain. **(C)** Focused classification of the extra densities revealed two conformations
529 for the-fold Fab on IgG3 bound DENV2, consistent with two alternate bivalent interactions
530 provided by the IgG3 Fc linker reach. **(D)** Spatial arrangement of the Fab densities on the two
531 conformations. Distances between the Glu216 (Eu numbering) residues in the HC CH1 are
532 shown for all potential bivalent interactions that could be mediated by a single mAb.

533 **Table 1: Comparison of immunogenetic features of conformational E-protein dimer**
534 **epitope antibodies to 3A06.**

		Heavy Chain V-gene					Light Chain V-gene			
Epitope	mAb ID	V-gene	D-gene	J-gene	SHM%	CDRH3 sequence	V-gene	J-gene	SHM%	CDRL3 sequence
	33.3A06	IGHV4-61*01	IGHD4-17*01	IGHJ5*01	11.34	TRMRGYGDYGARFTWLDS	IGLV1-44*01	IGLJ3*02	6.32	STWDDSLNGWV
EDE1	EDE1-C8	IGHV3-64D*06	IGHD2-21*01	IGHJ6*02	6.94	VGGYSNFYYYYTMDV	IGKV3-11*01	IGKJ2*01	5.02	QQRYNWPPYT
	EDE1-C10	IGHV1-3*01	IGHD4-17*01	IGHJ4*02	2.78	ARDKVDDYGDYWFPTLWYFDY	IGLV2-14*01	IGLJ3*02	3.82	SSHTSRGTWV
EDE2	EDE2-B7	IGHV3-74*01	IGHD3-22*01	IGHJ6*02	6.94	ARDGVRYYYDSTGYYPDNFFQYGLDV	IGLV2-23*01	IGLJ3*02	4.51	CSYAGGKSLV
	EDE2-A11	IGHV3-74*01	IGHD3-22*01	IGHJ6*02	8.68	VRDGVRFYYDSTGYYPDSFFKYGMDV	IGLV2-23*01	IGLJ3*02	6.94	CSYATSRTLV
Quaternary	SIgN-3C	IGHV1-46*01	IGHD3-22*01	IGHJ5*01	12.4	ARGGRALFYDSYTTPRDGGSWWFDP	IGKV1-33*01	IGKJ5	8.51	QQFDDLPIT

535

536 **REFERENCES**

537 1. Bhatt, S., Gething, P.W., Brady, O.J., Messina, J.P., Farlow, A.W., Moyes, C.L., Drake,
538 J.M., Brownstein, J.S., Hoen, A.G., Sankoh, O., et al. (2013). The global distribution and
539 burden of dengue. Nature *496*, 504–507. https://doi.org/10.1038/nature12060.

540 2. Aggarwal, C., Ahmed, H., Sharma, P., Reddy, E.S., Nayak, K., Singla, M., Maheshwari,
541 D., Chawla, Y.M., Panda, H., Rai, R.C., et al. (2024). Severe disease during both primary
542 and secondary dengue virus infections in pediatric populations. Nat Med *30*, 670–674.
543 https://doi.org/10.1038/s41591-024-02798-x.

544 3. Rouvinski, A., Dejnirattisai, W., Guardado-Calvo, P., Vaney, M.-C., Sharma, A., Duquerroy,
545 S., Supasa, P., Wongwiwat, W., Haouz, A., Barba-Spaeth, G., et al. (2017). Covalently
546 linked dengue virus envelope glycoprotein dimers reduce exposure of the
547 immunodominant fusion loop epitope. Nat Commun *8*, 15411.
548 https://doi.org/10.1038/ncomms15411.

549 4. Slon-Campos, J.L., Dejnirattisai, W., Jagger, B.W., López-Camacho, C., Wongwiwat, W.,
550 Durnell, L.A., Winkler, E.S., Chen, R.E., Reyes-Sandoval, A., Rey, F.A., et al. (2019). A
551 protective Zika virus E-dimer-based subunit vaccine engineered to abrogate antibody-
552 dependent enhancement of dengue infection. Nat Immunol *20*, 1291–1298.
553 https://doi.org/10.1038/s41590-019-0477-z.

554 5. Dejnirattisai, W., Wongwiwat, W., Supasa, S., Zhang, X., Dai, X., Rouvinski, A.,
555 Jumnainsong, A., Edwards, C., Quyen, N.T.H., Duangchinda, T., et al. (2015). A new class
556 of highly potent, broadly neutralizing antibodies isolated from viremic patients infected
557 with dengue virus. Nat Immunol *16*, 170–177. https://doi.org/10.1038/ni.3058.

558 6. Barba-Spaeth, G., Dejnirattisai, W., Rouvinski, A., Vaney, M.-C., Medits, I., Sharma, A.,
559 Simon-Lorière, E., Sakuntabhai, A., Cao-Lormeau, V.-M., Haouz, A., et al. (2016).
560 Structural basis of potent Zika-dengue virus antibody cross-neutralization. Nature *536*,
561 48–53. https://doi.org/10.1038/nature18938.

562 7. Priyamvada, L., Quicke, K.M., Hudson, W.H., Onlamoon, N., Sewatanon, J., Edupuganti,
563 S., Pattanapanyasat, K., Chokephaibulkit, K., Mulligan, M.J., Wilson, P.C., et al. (2016).
564 Human antibody responses after dengue virus infection are highly cross-reactive to Zika
565 virus. Proceedings of the National Academy of Sciences *113*, 7852–7857.
566 https://doi.org/10.1073/pnas.1607931113.

567 8. Dai, L., Xu, K., Li, J., Huang, Q., Song, J., Han, Y., Zheng, T., Gao, P., Lu, X., Yang, H., et
568 al. (2021). Protective Zika vaccines engineered to eliminate enhancement of dengue
569 infection via immunodominance switch. Nat Immunol *22*, 958–968.
570 https://doi.org/10.1038/s41590-021-00966-6.

571 9. Kudlacek, S.T., Metz, S., Thiono, D., Payne, A.M., Phan, T.T.N., Tian, S., Forsberg, L.J.,
572 Maguire, J., Seim, I., Zhang, S., et al. (2021). Designed, highly expressing, thermostable
573 dengue virus 2 envelope protein dimers elicit quaternary epitope antibodies. Sci Adv *7*,
574 eabg4084. https://doi.org/10.1126/sciadv.abg4084.

575 10. Kuhn, R.J., Zhang, W., Rossmann, M.G., Pletnev, S.V., Corver, J., Lenches, E., Jones,
576 C.T., Mukhopadhyay, S., Chipman, P.R., Strauss, E.G., et al. (2002). Structure of dengue
577 virus: implications for flavivirus organization, maturation, and fusion. Cell *108*, 717–725.
578 https://doi.org/10.1016/s0092-8674(02)00660-8.

579 11. Zhang, X., Sheng, J., Plevka, P., Kuhn, R.J., Diamond, M.S., and Rossmann, M.G. (2013).
580 Dengue structure differs at the temperatures of its human and mosquito hosts.
581 Proceedings of the National Academy of Sciences *110*, 6795–6799.
582 https://doi.org/10.1073/pnas.1304300110.

583 12. Priyamvada, L., Cho, A., Onlamoon, N., Zheng, N.-Y., Huang, M., Kovalenkov, Y.,
584 Chokephaibulkit, K., Angkasekwinai, N., Pattanapanyasat, K., Ahmed, R., et al. (2016). B
585 Cell Responses during Secondary Dengue Virus Infection Are Dominated by Highly
586 Cross-Reactive, Memory-Derived Plasmablasts. J Virol *90*, 5574–5585.
587 https://doi.org/10.1128/JVI.03203-15.

588 13. Rouvinski, A., Guardado-Calvo, P., Barba-Spaeth, G., Duquerroy, S., Vaney, M.-C., Kikuti,
589 C.M., Navarro Sanchez, M.E., Dejnirattisai, W., Wongwiwat, W., Haouz, A., et al. (2015).
590 Recognition determinants of broadly neutralizing human antibodies against dengue
591 viruses. Nature *520*, 109–113. https://doi.org/10.1038/nature14130.

592 14. Abbink, P., Larocca, R.A., Dejnirattisai, W., Peterson, R., Nkolola, J.P., Borducchi, E.N.,
593 Supasa, P., Mongkolsapaya, J., Screaton, G.R., and Barouch, D.H. (2018). Therapeutic
594 and protective efficacy of a dengue antibody against Zika infection in rhesus monkeys.
595 Nat Med *24*, 721–723. https://doi.org/10.1038/s41591-018-0056-0.

596 15. Fernandez, E., Dejnirattisai, W., Cao, B., Scheaffer, S.M., Supasa, P., Wongwiwat, W.,
597 Esakky, P., Drury, A., Mongkolsapaya, J., Moley, K.H., et al. (2017). Human antibodies to

598 the dengue virus E-dimer epitope have therapeutic activity against Zika virus infection.
599 Nat Immunol *18*, 1261–1269. https://doi.org/10.1038/ni.3849.

600 16. Sharma, A., Zhang, X., Dejnirattisai, W., Dai, X., Gong, D., Wongwiwat, W., Duquerroy,
601 S., Rouvinski, A., Vaney, M.-C., Guardado-Calvo, P., et al. (2021). The epitope
602 arrangement on flavivirus particles contributes to Mab C10's extraordinary neutralization
603 breadth across Zika and dengue viruses. Cell *184*, 6052-6066.e18.
604 https://doi.org/10.1016/j.cell.2021.11.010.

605 17. Hardy, J.M., Newton, N.D., Modhiran, N., Scott, C.A.P., Venugopal, H., Vet, L.J., Young,
606 P.R., Hall, R.A., Hobson-Peters, J., Coulibaly, F., et al. (2021). A unified route for flavivirus
607 structures uncovers essential pocket factors conserved across pathogenic viruses. Nat
608 Commun *12*, 3266. https://doi.org/10.1038/s41467-021-22773-1.

609 18. Hobson-Peters, J., Harrison, J.J., Watterson, D., Hazlewood, J.E., Vet, L.J., Newton, N.D.,
610 Warrilow, D., Colmant, A.M.G., Taylor, C., Huang, B., et al. (2019). A recombinant platform
611 for flavivirus vaccines and diagnostics using chimeras of a new insect-specific virus.
612 Science Translational Medicine *11*, eaax7888.
613 https://doi.org/10.1126/scitranslmed.aax7888.

614 19. Bibby, S., Jung, J., Low, Y.S., Amarilla, A.A., Newton, N.D., Scott, C.A.P., Balk, J., Ting,
615 Y.T., Freney, M.E., Liang, B., et al. (2025). A single residue in the yellow fever virus
616 envelope protein modulates virion architecture and antigenicity. Nat Commun *16*, 8449.
617 https://doi.org/10.1038/s41467-025-63038-5.

618 20. Martin Beem, J.S., Venkatayogi, S., Haynes, B.F., and Wiehe, K. (2023). ARMADiLLO: a
619 web server for analyzing antibody mutation probabilities. Nucleic Acids Research *51*,
620 W51–W56. https://doi.org/10.1093/nar/gkad398.

621 21. Boesch, A.W., Miles, A.R., Chan, Y.N., Osei-Owusu, N.Y., and Ackerman, M.E. (2017).
622 IgG Fc variant cross-reactivity between human and rhesus macaque FcγRs. mAbs *9*,
623 455–465. https://doi.org/10.1080/19420862.2016.1274845.

624 22. Xu, L., Kumar, S., Moore, K.M., Vander Velden, J.W., Mbadugha, F.A., Wang, M.,
625 Hailstorks, T., Sundberg, E.J., Sastre, D.E., Suthar, M.S., et al. (2025). FcγRI is the key
626 determinant of antibody-mediated Zika virus infection of human placental macrophages.
627 bioRxiv, 2025.10.23.684201. https://doi.org/10.1101/2025.10.23.684201.

628 23. Lim, X.-X., Shu, B., Zhang, S., Tan, A.W.K., Ng, T.-S., Lim, X.-N., Chew, V.S.-Y., Shi, J.,
629 Screaton, G.R., Lok, S.-M., et al. (2021). Human antibody C10 neutralizes by diminishing
630 Zika but enhancing dengue virus dynamics. Cell *184*, 6067-6080.e13.
631 https://doi.org/10.1016/j.cell.2021.11.009.

632 24. Saunders, K.O. (2019). Conceptual Approaches to Modulating Antibody Effector
633 Functions and Circulation Half-Life. Front Immunol *10*, 1296.
634 https://doi.org/10.3389/fimmu.2019.01296.

635 25. Schlothauer, T., Herter, S., Koller, C.F., Grau-Richards, S., Steinhart, V., Spick, C.,
636 Kubbies, M., Klein, C., Umaña, P., and Mössner, E. (2016). Novel human IgG1 and IgG4
637 Fc-engineered antibodies with completely abolished immune effector functions. Protein
638 Eng Des Sel *29*, 457–466. https://doi.org/10.1093/protein/gzw040.

639 26. Scott, C.A.P., Amarilla, A.A., Bibby, S., Newton, N.D., Hall, R.A., Hobson-Peters, J., Muller,
640 D.A., Chappell, K.J., Young, P.R., Modhiran, N., et al. (2021). Implications of Dengue Virus
641 Maturation on Vaccine Induced Humoral Immunity in Mice. Viruses *13*.
642 https://doi.org/10.3390/v13091843.

643 27. Newton, N.D., Hardy, J.M., Modhiran, N., Hugo, L.E., Amarilla, A.A., Bibby, S., Venugopal,
644 H., Harrison, J.J., Traves, R.J., Hall, R.A., et al. (2021). The structure of an infectious
645 immature flavivirus redefines viral architecture and maturation. Science Advances *7*,
646 eabe4507. https://doi.org/10.1126/sciadv.abe4507.

647 28. Djender, S., Beugnet, A., Schneider, A., and Marco, A.D. (2014). The Biotechnological
648 Applications of Recombinant Single-Domain Antibodies are Optimized by the C-Terminal
649 Fusion to the EPEA Sequence (C Tag). Antibodies *3*, 182–191.
650 https://doi.org/10.3390/antib3020182.

651 29. De Genst, E.J., Guilliams, T., Wellens, J., O'Day, E.M., Waudby, C.A., Meehan, S.,
652 Dumoulin, M., Hsu, S.-T.D., Cremades, N., Verschueren, K.H.G., et al. (2010). Structure
653 and Properties of a Complex of α-Synuclein and a Single-Domain Camelid Antibody.
654 Journal of Molecular Biology *402*, 326–343. https://doi.org/10.1016/j.jmb.2010.07.001.

655 30. Yonekura, K., Maki-Yonekura, S., Naitow, H., Hamaguchi, T., and Takaba, K. (2021).
656 Machine learning-based real-time object locator/evaluator for cryo-EM data collection.
657 Commun Biol *4*, 1044. https://doi.org/10.1038/s42003-021-02577-1.

31. Grant, T., Rohou, A., and Grigorieff, N. (2018). cisTEM, user-friendly software for single-particle image processing. eLife *7*, e35383. https://doi.org/10.7554/eLife.35383.

32. Jung, J., Grant, T., Thomas, D.R., Diehnelt, C.W., Grigorieff, N., and Joshua-Tor, L. (2019). High-resolution cryo-EM structures of outbreak strain human norovirus shells reveal size variations. Proceedings of the National Academy of Sciences *116*, 12828–12832. https://doi.org/10.1073/pnas.1903562116.

33. Croll, T.I. (2018). ISOLDE: a physically realistic environment for model building into low-resolution electron-density maps. Acta Cryst D *74*, 519–530. https://doi.org/10.1107/S2059798318002425.

34. Emsley, P., Lohkamp, B., Scott, W.G., and Cowtan, K. (2010). Features and development of Coot. Acta Cryst D *66*, 486–501. https://doi.org/10.1107/S0907444910007493.

35. Afonine, P.V., Poon, B.K., Read, R.J., Sobolev, O.V., Terwilliger, T.C., Urzhumtsev, A., and Adams, P.D. (2018). Real-space refinement in PHENIX for cryo-EM and crystallography. Acta Cryst D *74*, 531–544. https://doi.org/10.1107/S2059798318006551.

36. Lefranc, M.-P., Giudicelli, V., Ginestoux, C., Jabado-Michaloud, J., Folch, G., Bellahcene, F., Wu, Y., Gemrot, E., Brochet, X., Lane, J., et al. (2009). IMGT, the international ImMunoGeneTics information system. Nucleic Acids Res. *37*, D1006-1012. https://doi.org/10.1093/nar/gkn838.

37. Giudicelli, V., Brochet, X., and Lefranc, M.-P. (2011). IMGT/V-QUEST: IMGT standardized analysis of the immunoglobulin (IG) and T cell receptor (TR) nucleotide sequences. Cold Spring Harb Protoc *2011*, 695–715. https://doi.org/10.1101/pdb.prot5633.